Automating 3D Surgical Suture Planning

Viraj Ramakrishnan*[1], Julia Isaac*[1], Harshika Jalan[1], Harsha Polavaram[1],
Aviv Adler[1], Hansoul Kim[1], Danyal M Fer[2], Ken Goldberg[1]

***Abstract*— In surgical practice, precise and careful suture placement can reduce scarring and speed healing. Surgeons rely on expertise to guide where they place suture needle entry and exit points, but the complexity of wound geometry and tissue dynamics makes it challenging for even experienced surgeons to select suture placement. We extend our previous 2D suture planning algorithm with SP3DEEF: Suture Planning 3D Equalizing Elliptical Forces, an algorithm that outputs an optimized suture plan considering forces acting on the wound and surrounding tissue in 3D. In physical experiments with raw chicken thighs, SP3DEEF was able to generate suture plans that meet all specifications in under 60 seconds. When manually executed with a surgical needle by an untrained engineering student, the resulting suture plans completely closed all wounds with little buckling or gaps.**

I. Introduction

Suturing is a critical task in surgical procedures in which tissue edges are approximated using thread [1]. The points of surgical needle entry and exit define a *suture plan*. A suture plan involves many trade-offs. For example, placing sutures too close together can disrupt blood flow, but too much separation will not properly bind the wound together [2]. Depending on the spacing of sutures, patients suffer scars, with symptoms including changes in color, hardness, and itchiness, reported via the POSAS scale, a metric used to evaluate scar quality. [2]. Suture placement also affects the rate of complications post-surgery. Sutures exert forces on the surrounding tissue, causing the deformation of the surrounding skin. Improper tension in the sutures can lead to infection or ischemic necrosis [3].

We extend our previous paper and SP2DEEF [4] and present a 3D automated suture placement methodology, SP3DEEF: Suture Planning 3D Equalizing Elliptical Forces, an algorithm designed to generate an optimized 3D suture plan, by following clinical guidelines and considering the forces acting on the surrounding tissue. Wounds might not lie on a part of the skin that is flat or orientable to be parallel to a camera. In such cases, modeling the wound in 3D is important to overcome perspective effects that are introduced by projecting to 2D. Our previous paper [4] assumed that the surgeon would provide points along a line representing the wound. We relax this assumption by identifying the location of the wound using Computer Vision.

This paper makes three contributions:

1) The first application of Meta's Segment Anything Model (SAM) [5] to segment a human wound in an image.
2) Extension of the SP2DEEF algorithm to compute suture plans for non-linear wounds in 3D.
3) Physical experiments suggesting that the algorithm is able to generate suture plans that meet specified spacing criteria.

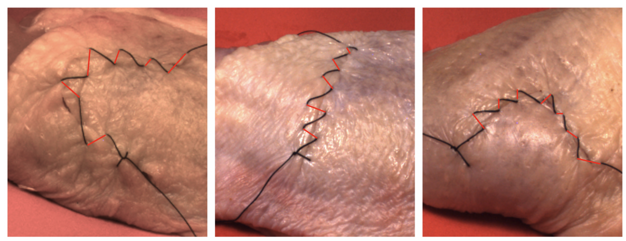

Fig. 1: Algorithm outputs for wounds on curved 3D surfaces.

II. Related Work

Suture planning from images can be divided into four stages: Wound Segmentation, 3D Tissue Modeling, 3D Suture Planning, and 3D Needle Path Planning. Building on our previous paper, Kamat et al. [6], this paper focuses on the first three stages of this process and extends it to 3D wounds.

A. Wound Segmentation

Segmenting wounds from images is challenging due to the diverse shapes, colors, body positions, background compositions and camera qualities. State-of-the-art methods for wound image segmentation use machine learning techniques, including supervised and unsupervised classification and deep learning. Wang et al. [7] apply SVM based classifiers to determine wound boundaries in images. Scebba et al. [8] employed two deep-learning architectures to detect and segment wounds and tested their performance on diabetic foot ulcer images. Wang et al. [9] utilized the ConvNet, based on an encoder–decoder CNN architecture, for wound segmentation, infection detection, and healing progress prediction. Meta's Segment Anything Model (SAM) is a zero-shot learning algorithm for segmenting user-defined objects [5]. It allows various interactive prompts, such as points or a bounding box, and produces object masks on various segmentation tasks. Previous studies by Wu et al. [10] have adapted the Segment Anything Model for medical image segmentation tasks spanning different modalities such as multi-organ segmentation, brain tumor segmentation from MRI images and melanoma segmentation from tissue images.

[1] The AUTOLAB at the University of California, Berkeley (`automation.berkeley.edu`)
[2] MD, Department of Surgery, Emory School Of Medicine
* Denotes equal contribution

However, we believe ours is the first paper to apply SAM to wound segmentation.

B. 3D Tissue Modeling

Previous studies have used Finite Element Modelling to simulate the behavior of human tissue during suturing. Lapeer et al. [11] present a finite element model of human tissue suitable for use in a real-time computer-based simulator to teach surgeons procedures, such as facial reconstruction using tissue-flap repair. Yoshida et al. [12] propose a surgical simulation system of tissue sutures using a 3D finite element method developed from point clouds obtained with a 3D surface measuring device. A surgeon can use the simulation system to evaluate an appropriate suturing method to reduce postoperative tissue extrusions. FEMs have also been developed to study the effect of different surgical excision shapes on wound closure mechanics [13].

C. 3D Suture Planning

3D suture placement models aim to represent the mechanics of wound closure more realistically than 2D models. Chanda et al. [14] developed a 3D computational model of the tissue with two layers and placed interrupted sutures to close a diamond shaped wound with varying cross section. The force requirements for each suture were estimated numerically using a novel suture pulling technique and were found to be 0–5 N with a maximum value at the center. Kam et al. [15] present a 3D path planning algorithm to enable semi-autonomous robotic anastomosis on animal tissue. The algorithm generates a suture placement plan based on the locations of 3D near infrared markers and updates the plan after each completed stitch using a non-rigid registration technique. 3D force optimization has other clinical applications besides suturing. Patil et al. [16] proposed a method to optimize the curvature and torsion along three dimensional channels or ribbons designed for intracavity brachytherapy. One can view the ribbons, a surface that follows the path of the wound, lying on the surface of the tissue, as a model of the local area around the wound. Thus, suture placement can be imagined as placing sutures along the ribbon following the wound line.

D. 3D Needle Path Planning

The sub-task of planning how the suturing needle moves through tissue has also been researched extensively. Tissue occluding the needle and the deformable nature of the tissue make the task of moving the needle through the tissue challenging. Sen et al. [17] studied optimizing the needle size and trajectory using sequential convex programming. Schulman et al. [18] apply the transfer trajectory method and adapt it for needle path planning. In a similar vein, van den Berg et al. [19] explore knot tying, a sub-task in suturing for which 3D needle location is crucial. Schorp et al. [20] propose an interactive perception-based approach to tracking surgical thread in 3D and apply it to perform the suture "tail-shortening" task.

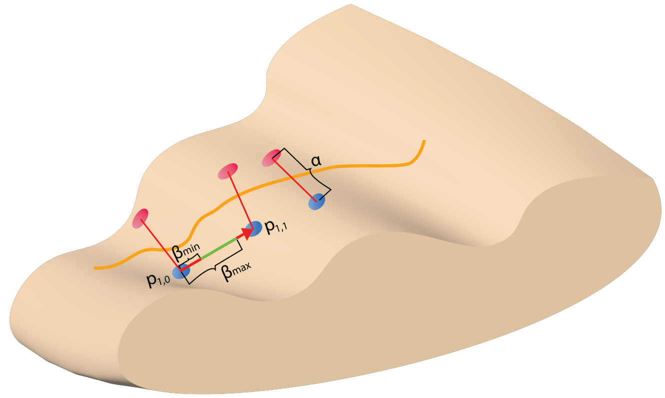

Fig. 2: **3D Distance Constraints.** A simulated wound in 3D, where the sutures placed at $p_{1,0}, p_{1,1}$ violate distance constraints. The wound spline is shown in red, with three insertion points (red) and three extraction points (blue). Here, α denotes the desired suture width, representing the Euclidean distance between entry and exit points perpendicular to the wound axis. γ is the ideal distance between sutures. The Euclidean distance between extraction points $p_{1,0}$ and $p_{1,1}$ falls outside the acceptable range defined by βmin and βmax, a violation of constraints. The arrow between $p_{1,0}, p_{1,1}$ is split into green (proper placements) and red (improper placements) segments.

III. Problem Statement

Given a 3D tissue surface with a single embedded wound, a thin contiguous area with no branches, we wish to find a suture plan satisfying certain constraints on suture point distances and imparting forces on the wound which close the wound well while minimizing disruptive shear forces (or report that no such placement exists). We formulate this as a constrained optimization problem.

Assumptions: We assume that two images of the wound are taken from two RGB cameras, forming a stereo camera system, with known intrinsics, in a well-lit environment [21], and that the wound is fully visible from both cameras and is not occluded by other body parts. We assume that the wound does not branch, and can thus be approximated as a spline in x, y, z space, and that the surface immediately around the wound can be estimated locally as a 3D surface. We assume that blood has been cleaned from the surrounding skin to aid wound recognition.

Parameters and Hyperparameters: Adopting similar notation to our previous paper [4], consider the distance parameters displayed in Figure 2. We let the distance between the insertion and extraction points of a single suture be the *suture width*, denoted α. The point halfway between the insertion and extraction points, which lies on the wound, is referred to as the *wound point* of the suture. Let the *suture distance* be the Euclidean distance between two successive wound, insertion or extraction points. We denote the ideal suture distance as γ and set it to 5mm. This parameter can be adjusted at the surgeon's preference. We constrain that the distance between any two sutures must be more than β_{min} and the distance between any two consecutive sutures be less than β_{max}, and we denote these constraints as A_{min} and A_{max}. These constraints force the suturing plan to meet surgical guidelines, informed by clinical expertise.

Loss Function: We define our loss function to be the

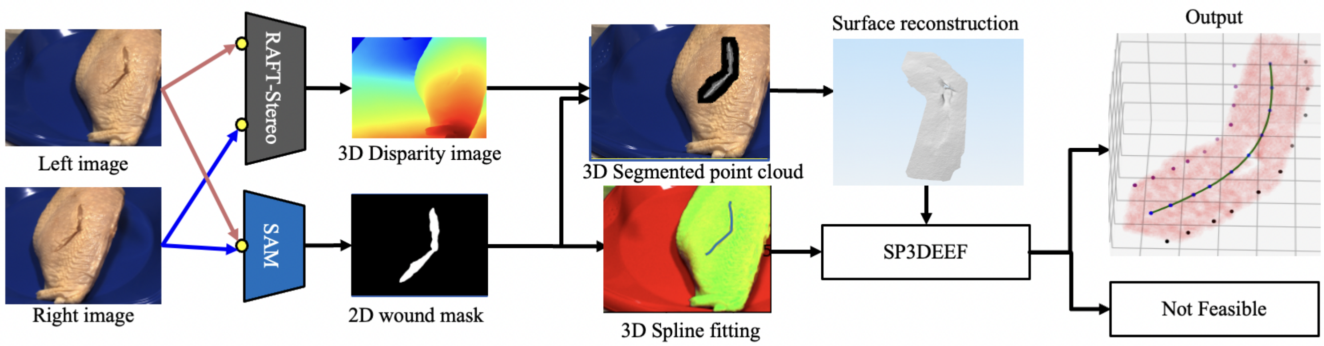

Fig. 3: **Suture Planning 3D Equalizing Elliptical Forces (SP3DEEF).** The inputs (shown at left) are the images captured by the left and right cameras; the wound area is segmented out via SAM and points are converted to a disparity image via RAFT-STEREO to produce a segmented 3D point cloud from which the tissue surface is reconstructed. Finally, the 2D wound mask is used to fit a 3D spline (green) and optimizes the rest of suture placement over the reconstructed surface. SP3DEEF outputs the full suture plan overlaid on the original wound image (right).

weighted sum of separate loss functions. L_d is the Mean Squared Error (MSE) of the suture distances of the wound points from γ, measuring deviation from the ideal suture distance, and c_d is the weight of this loss. Let L_i, L_w and L_e be the variance in suture distances of, respectively, the insertion points, wound points and extraction points; let c_i, c_w, and c_e be the corresponding weights in the overall loss function, which were set based on surgical advice about the relative importance of each of these factors. Given the insertion and extraction points, our force model predicts the forces that each suture will impart on the wound. We consider the sum of all the forces acting on a particular point on the wound line, and we project the force onto the directions parallel and perpendicular to the wound. We denote the force perpendicular to the wound line as the *closure force* and the force acting along the wound line as *shear force*. Let the MSE of the closure forces from an ideal value be L_f, and let the average squared shear force be L_s, with associated weights c_f and c_s.

Variables: Let n be the number of sutures that the final suture plan has. Although, strictly speaking, this stays constant during the optimization, we attempt optimization for a range of values, based on the dimensions of the wound. Additionally, let ℓ be the length of the wound. Consider a spline, $P(s)$, fit to the shape of the wound, parameterized by a single variable, s, such that $s = 0$ at the start of the spline, and $s = 1$ at the end. In this formulation of the problem, we set the initial insertion and extraction points to be $\frac{\alpha}{2}$ away, in directions perpendicular to the spline. Thus, we can specify the position of the sutures entirely with the position of the wound points along the spline. Hence, the wound points are the decision variables over which we optimize. Specifically, this paper considers s_i, for $i \in [0, n)$, with $0 \le s_0 \le s_1 \ldots \le s_{n-1} \le 1$, such that $P(s_i)$ yields the i^{th} wound point.

Outputs: The system outputs an ordered list of insertion and extraction points, $p_{0,i}$ and $p_{1,i}$, projecting them back onto the 3D surface for the surgeon to reference. The algorithm outputs the loss associated with the placement with lowest loss. If the suture plan violates any of the constraints set out in the problem, this is considered a termination.

Objective:

The optimization problem is given by:

$$\begin{aligned} \min_{\{s_0,\ldots,s_{n-1}\}} \quad & c_d L_d + c_i L_i + c_w L_w + c_e L_e + c_f L_f + c_s L_s \\ \text{s.t.} \quad & A_{\min},\ A_{\max},\quad 0 \le s_0 \le \cdots \le s_{n-1} \le 1 \end{aligned} \tag{1}$$

IV. Methodology

The SP3DEEF algorithm is an extension of the SP2DEEF algorithm from [4] to 3D, along with additional automation (specifically of identifying the wound trajectory). The algorithm can be split into the following phases:

A. *2D Mask Generation*: using our input of a stereo pair of images of the wound, Meta's Segment Anything Model (SAM) is used to segment the wound area.
B. *3D Transformation*: RAFT-STEREO [22] is used to generate a 3D model of the ribbon and surrounding wound area from the pair of masks, and a mesh is created represent the surface.
C. *Spline Fitting*: a spline in 3D is used to geometrically define the suture area of segmented wounds, insertion points, and extraction points as three parallel 3D splines.
D. *Optimization*: the system plans the placement of sutures along the ribbon representing the wound, subject to constraints and objective function, by estimating the forces that the tissue is experiencing.
E. *Adjustment*: the surgeon is shown the suture plan and can make final adjustments as desired.

A. 2D Mask Generation

SAM is used to segment the wound area in the entire image. SAM has various prompts to assist in identifying the wound's location, including indicating the image's foreground and background and selecting a rectangular portion of the image for segmentation. We fed the images with bounding boxes indicating the wound region into SAM, using the SAM ViT-B model checkpoint, available at: https://github.com/facebookresearch/segment-anything, using a 8GB 2022 M2 MacBook Air for inference.

B. 3D Transformation

RAFT-STEREO is used to transform the 2D geometric information of wounds in the image into 3D, using a disparity image generated from a pair of images. We apply the mask generated by SAM to filter out the non-wound areas from the disparity image. Then, the intrinsic and extrinsic matrices of camera, along with the segmented disparity image, are used to make a 3D pointcloud [22], and the CGAL implementation of Advancing Front Surface Reconstruction [23] is used to produce a mesh.

C. Spline Fitting

To fit the wound spline, having extracted the mask from both views, the left mask is picked arbitrarily. Firstly, we retain the largest connected component of the mask, to prevent noise from affecting the spline. We then dilate the mask with a kernel of 5 pixels, meaning that all pixels within a 5 pixel radius of the mask are included in the new mask. We fill in the holes in the mask that might interfere with spline detection. We then skeletonize the image using a method from [24] to reduce the mask to a single pixel wide. To fit a spline to these points, we need to prune extraneous branches and order the points along the wound. We construct a graph where adjacent pixels in the mask have edges between them and then find the longest path in the resulting graph which yields a branch-free ordered set of points along the wound. We then interpolate a spline to fit these points based on the method presented in [25], with smoothing applied to generate the spline.

Next, we formulate a ribbon, similar to [16], which follows the wound spline and lies on the wound surface. To fit splines to potential insertion and extraction points, we first sample points on the wound spline. For each sampled point $P(s_i)$, we consider the derivative of the wound spline at $P(s_i)$, $\frac{dP}{ds}(s_i)$. We then sample the nearest 100 points lying on the mesh, which gives us a good approximation of the surface close to $P(s_i)$, and use least squares to fit a local plane to the surface. Then, we take the cross product of the normal of the plane and the derivative vector to get a vector that lies on the plane, but is also perpendicular to the spline. We follow the vector in both directions at a distance of $\alpha/2$ to generate the insertion and extraction points. Note that this procedure results in sutures that are perpendicular to the wound, with insertion and extraction points at a distance of $\alpha/2$ away from the wound, as required. Using these generated points, we fit two more smoothed splines using `scipy.interpolate.UnivariateSpline`.

D. Optimization

It is important that forces acting to bring the two sides of the wound together be consistent, sufficient to close the wound but not too great to cause adverse effects [26]. Additional factors such as the proximity of insertion and extraction points to each other are also important to patient recovery.

SP3DEEF extends SP2DEEF [6] to the case of a curved wound on a curved surface in 3D. In particular, we assume the wound is a 1D curved spline on a 2D manifold embedded in 3D space. The SP3DEEF optimization problem is non-convex, hence we use the Sequential Least Squares Programming algorithm [27] as an efficient way to optimize a non-convex objective function over few variables. To explore a range of values for n (the number of sutures), we first approximate the optimal number of sutures by $\hat{n} = \lfloor \frac{\ell}{\gamma} \rfloor$, as SP2DEEF did, and then proceed to perform optimization for integer $n \in [0.5 * \hat{n}, 1.4 * \hat{n}]$. This range of values allows us to test a variety of suture plans and select the one that has the minimum loss without being too computationally expensive.

Suture Regularity: To ascertain suturing distances, we must first determine how to place the insertion and extraction points, given the i^{th} wound point, that is, $P(s_i)$. We use the insertion and extraction spline to calculate the corresponding locations of the insertion and extraction points. Letting $p_{0,i}$ and $p_{1,i}$ be the i^{th} insertion and extraction points, our constraints are as follows: $\beta_{\min} \leq \|p_{0,i} - p_{1,i}\| < \beta_{\max}$, and that $p_{0,i} - p_{1,i}$ does not cross $p_{0,j} - p_{1,j}$ for any $i \neq j$. As in [4], we add 'phantom' sutures at the start and end of the wound, denoted $s_{-1} = 0, s_n = 1$. The distance and variance loss terms are:

$$L_{\mathrm{d}}(s_0, \ldots, s_{n-1}) = \frac{1}{n+1} \sum_{i=-1}^{n-1} (\|P(s_{i+1}) - P(s_i)\| - \gamma)^2 \quad (2)$$

$$L_i(s_0, \ldots, s_{n-1}) = \mathrm{Var}\big(\{\|P(s_{i+1}) - P(s_i)\|\}_{i=-1}^{n-1}\big) \quad (3)$$

with L_e and L_w being calculated identically to L_i, except with the extraction and wound points rather than insertion points.

Elliptical Forces: To obtain estimates for forces along the wound, we must develop a model of how forces propagate through tissue. When the wound is a straight line and lies on a planar surface, a useful model of force distribution is the *Diamond Force Model* [28]. In the Diamond Force Model, the force imparted by a single suture is at a maximum where the suture intersects the wound, and decreases linearly to zero as you move along the wound away from the suture. However, this formulation requires extension for non-linear wounds.

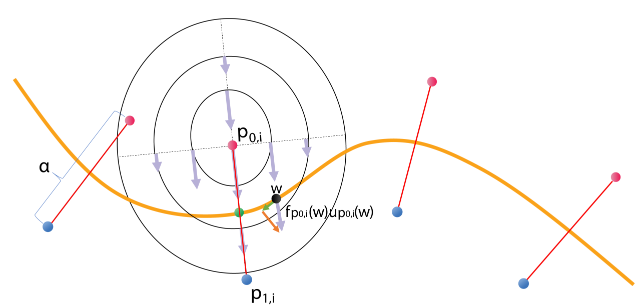

Fig. 4: **SP2DEEF (Elliptical Force) Model.** The SP2DEEF model applied to sutures of width α around insertion point $p_{0,i}$ is shown as a region of nonzero force imparted from $p_{0,i}$, with forces decreasing linearly from the center, with elliptical isocontours. Green and orange arrows represent shear and closure forces generated at the wound point w by $p_{0,i}$.

In our previous paper, we proposed the SP2DEEF (Elliptical Force) Model, depicted in Figure 4. A suture is considered to impart forces on the skin from the insertion and extraction points, which pushes the wound closed from both sides. The magnitude of the force decays linearly in both the direction parallel and perpendicular to the suture; as in the Diamond Force Model, the forces imparted by a given suture are always parallel to it. This creates concentric ellipses of equal force with the magnitude of the force decreasing linearly to zero as the ellipses get further out. For each point on the wound, the total insertion force is the sum of the forces imparted on it from insertion points; likewise, the total extraction force is the sum of forces imparted on it from the extraction points. The interaction between the total insertion force and total extraction force then produces the closure and shear forces (respectively, perpendicular and parallel to the wound). However, allowing the surface of the tissue to exist in 3D adds extra complications.

To compute the force that a single insertion point $p_{0,i}$ exerts on a wound point w, we need to know: (a) the angle of the force at w; (b) the magnitude of the force at w. We first calculate the angle at which the force is felt. We find the vector, $\vec{c}$ from $p_{0,i}$ to w on the mesh representing the surface. We project this vector onto the tangent planes of the surface at $p_{0,i}$ and w. Then the angle θ between $\vec{c}$ and the direction of the suture (given by $p_{1,i} - p_{0,i}$, projected onto the tangent plane at $p_{0,i}$) is computed; the force felt at w is then at an angle of θ from $\vec{c}$. We denote the direction of the force imparted by $p_{0,i}$ on w as $u_{p_{0,i}}(w)$. The distance between w and $p_{0,i}$ is then the Euclidean distance in 3D. Given this distance $\|w - p_{0,i}\|$ and angle θ, the magnitude of the force $f_{p_{0,i}}(w)$ is computed as in the elliptical force model from [4]:

$$f_{p_{0,i}}(w) = \max(\eta - \|w - p_{0,i}\| \sqrt{\cos(\theta)^2 + \xi^2 \sin(\theta)^2}, 0) \quad (4)$$

where η is the maximum force from a single suture (felt at $p_{0,i}$ itself) and $\xi > 0$ is the ratio of the force ellipse's axes.

To calculate the total force felt at a point $w = P(s)$ on the wound, the total insertion and extraction forces are computed:

$$F_{in}(s) = \sum_{i=0}^{n-1} f_{p_{0,i}}(w) u_{p_{0,i}}(w) \quad (5)$$

$$F_{ex}(s) = \sum_{i=0}^{n-1} f_{p_{1,i}}(w) u_{p_{1,i}}(w) \quad (6)$$

The total force experienced in bringing the wound together at $w = P(s)$ is then $F_{in}(s) - F_{ex}(s)$. Let the normalized tangent of the wound at w be $\frac{dP}{ds}|_s$, and the normalized vector perpendicular to the spline be $P_{norm}|_s$. Then,

$$F_{shr}(s) = (F_{in}(s) - F_{ex}(s))^\top \frac{dP}{ds}|_s \quad (7)$$

$$F_{cls}(s) = (F_{in}(s) - F_{ex}(s))^\top P_{norm}|_s \quad (8)$$

From here we calculate our closure and shear force losses. As shear forces act to pull the tissue away from its original position, the ideal amount of shear force is zero. For closure forces, we let the ideal amount of force, F_{idl} be the amount of force that a wound point would experience if it was held in place by sutures exactly γ away, on a straight wound. Assuming we choose m points along the spline to evaluate our closure and shear forces at $t_0, t_1, \ldots, t_{m-1}$, we have that

$$L_f = \frac{1}{m} \sum_{j=0}^{m-1} (F_{idl} - F_{cls}(t_j))^2 \quad (9)$$

$$L_s = \frac{1}{m} \sum_{j=0}^{m-1} F_{shr}(t_j)^2 \quad (10)$$

V. Physical Experiments

Two Allied Vision Prosilica GCX 1920 cameras were used to capture images. We experimented on chicken thigh skin, due to its similarity to human skin. A wound was made into the thigh with a scalpel. We indicated the location of the wound in both photos, and then fed the spline detected into 1) The SP2DEEF algorithm, 2) A baseline that equally spaced sutures in 3D, and 3) the SP3DEEF alogrithm. To compare all of the algorithms on equal footing, we projected the output of SP2DEEF into 3D, and calculated the loss that our 3D loss function estimated.

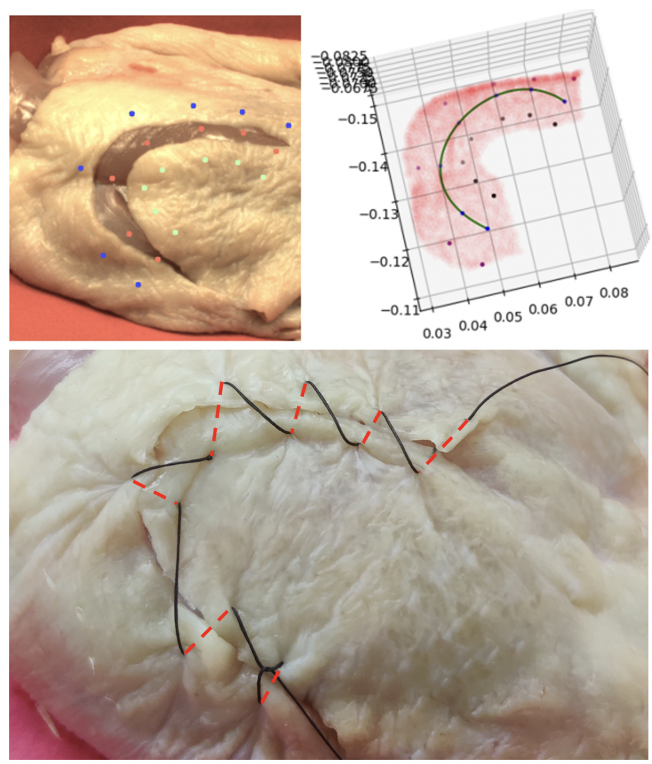

Fig. 5: **Example.** *Upper Left*: Image of a non-linear wound on fresh chicken skin. *Upper Right*: Output of SP3DEEF: suture needle entry and exit points *Bottom*: The executed suture plan. Note that the visible suture thread (above the skin) links the stiches (below the skin, shown in blue) which hold the wound close.

We analyzed three wounds. The SP3DEEF placement from the algorithm met all spacing conditions. Pushpins were used to indicate the location on the chicken of the insertion and extraction points. Then, the wound was sutured using USP Size 2-0 thread and GS-22 suturing needle. SP3DEEF suturing plans were able to achieve wound closure in all cases. An expert surgeon (Danyal Fer, Department of Surgery, Emory School of Medicine, with over 5000 hours of surgical experience) assessed that, given the ability to adjust the width of the sutures and the desired distance between sutures to what the wound necessitated, the resulting suture plans are appropriate.

The surgeon did make some comments on the placement generated for wound 3. In their assessment, a suture should have been placed directly in the corner, which SP3DEEF did not do. In addition, the spline was unable to fit well to the sharp corner of the wound, leading to the actual distance from the edge of the skin to the suture being too small.

VI. Conclusion

A. Limitations

This work has the following limitations:

- As we do not have authorization to perform live animal experiments, we do not have data on wound healing or POSAS scar assessment.
- As with previous work, the wound is represented as a spline in one variable, and cannot have any branches.
- We assume that a fixed α suffices for the whole wound. However, it might be the case that certain sections warrant sutures that are longer or shorter.
- Wound depth and variations in skin thickness and elasticity are not taken into account.
- Wound deformation during the suturing procedure is not considered.

B. Future work

We plan to perform more experiments and extend SP3DEEF with an interactive interface to facilitate surgeon modification of suture plans. To account for branching wounds, we will develop an algorithm that separately solves the branches, and intelligently combines the separate plans together. To account for wound deformation during suturing, we will develop a model that computes the next suture placement given a partially sutured wound, in response to wound deformation.

References

[1] K. Umakanth, M. Neralla, and D. Prabu, "Knowledge, awareness, and prevalence of various types of suturing techniques used for intraoral wound closure," *J. Adv. Pharm. Technol. Res.*, vol. 13, no. Suppl 1, pp. S259–S264, Nov. 2022.

[2] A. Stoecker, C. M. Blattner, S. Howerter, W. Fancher, J. Young, and W. Lear, "Effect of simple interrupted suture spacing on aesthetic and functional outcomes of skin closures," *Journal of Cutaneous Medicine and Surgery*, vol. 23, no. 6, pp. 580–585, 2019, pMID: 31272216.

[3] N. Marsidi, S. A. Vermeulen, T. Horeman, and R. E. Genders, "Measuring forces in suture techniques for wound closure," *Journal of Surgical Research*, vol. 255, pp. 135–143, 2020.

[4] V. Kamat, V. Ramakrishnan, Y. Mohnot, H. Jalan, J. Isaac, V. Schorp, Y. Avigal, A. Adler, D. M. Fer, and K. Goldberg, "Automating 2d suture placement," in *2023 IEEE 19th CASE*. IEEE, 2023, pp. 1–8.

[5] A. Kirillov, E. Mintun, N. Ravi, H. Mao, C. Rolland, L. Gustafson, T. Xiao, S. Whitehead, A. C. Berg, W.-Y. Lo, P. Dollár, and R. Girshick, "Segment anything," 2023.

[6] V. Kamat, V. Ramakrishnan, Y. Mohnot, H. Jalan, J. Isaac, V. Schorp, Y. Avigal, A. Adler, D. Fer, and K. Goldberg, "Automating 2d suture placement," *2023 IEEE 19th CASE*, pp. 1–8, 2023.

[7] L. Wang, P. C. Pedersen, E. Agu, D. M. Strong, and B. Tulu, "Area determination of diabetic foot ulcer images using a cascaded two-stage svm-based classification," *IEEE Transactions on Biomedical Engineering*, vol. 64, no. 9, pp. 2098–2109, 2017.

[8] G. Scebba, J. Zhang, S. Catanzaro, C. Mihai, O. Distler, M. Berli, and W. Karlen, "Detect-and-segment: A deep learning approach to automate wound image segmentation," *Informatics in Medicine Unlocked*, vol. 29, p. 100884, 2022.

[9] C. Wang, X. Yan, M. Smith, K. Kochhar, M. Rubin, S. M. Warren, J. Wrobel, and H. Lee, "A unified framework for automatic wound segmentation and analysis with deep convolutional neural networks," in *2015 37th Annual International Conference of the IEEE Engineering in Medicine and Biology Society (EMBC)*, 2015, pp. 2415–2418.

[10] J. Wu, W. Ji, Y. Liu, H. Fu, M. Xu, Y. Xu, and Y. Jin, "Medical sam adapter: Adapting segment anything model for medical image segmentation," 2023.

[11] R. J. Lapeer, P. D. Gasson, and V. Karri, "A hyperelastic finite-element model of human skin for interactive real-time surgical simulation," *IEEE Transactions on Biomedical Engineering*, vol. 58, no. 4, pp. 1013–1022, 2011.

[12] H. Yoshida, S. Tsutsumi, M. Mizunuma, and A. Yanai, "A surgical simulation system of skin sutures using a three-dimensional finite element method," *Clinical Biomechanics*, vol. 16, no. 7, pp. 621–626, 2001.

[13] C. Flynn, "Finite element models of wound closure," *Journal of Tissue Viability*, vol. 19, no. 4, pp. 137–149, 2010.

[14] A. Chanda and V. Unnikrishnan, "A realistic 3d computational model of the closure of skin wound with interrupted sutures," *Journal of Mechanics in Medicine and Biology*, vol. 17, no. 01, p. 1750025, 2017.

[15] M. Kam, H. Saeidi, S. Wei, J. D. Opfermann, S. Leonard, M. H. Hsieh, J. U. Kang, and A. Krieger, "Semi-autonomous robotic anastomoses of vaginal cuffs using marker enhanced 3d imaging and path planning," in *Medical Image Computing and Computer Assisted Intervention – MICCAI 2019*, D. Shen, T. Liu, T. M. Peters, L. H. Staib, C. Essert, S. Zhou, P.-T. Yap, and A. Khan, Eds. Cham: Springer International Publishing, 2019, pp. 65–73.

[16] S. Patil, J. Pan, P. Abbeel, and K. Goldberg, "Planning curvature and torsion constrained ribbons in 3d with application to intracavitary brachytherapy," *IEEE Transactions on Automation Science and Engineering*, vol. 12, no. 4, pp. 1332–1345, 2015.

[17] S. Sen, A. Garg, D. V. Gealy, S. McKinley, Y. Jen, and K. Goldberg, "Automating multi-throw multilateral surgical suturing with a mechanical needle guide and sequential convex optimization," in *2016 IEEE ICRA*, 2016, pp. 4178–4185.

[18] J. Schulman, A. Gupta, S. Venkatesan, M. Tayson-Frederick, and P. Abbeel, "A case study of trajectory transfer through non-rigid registration for a simplified suturing scenario," in *2013 IEEE/RSJ IROS*, 2013, pp. 4111–4117.

[19] J. van den Berg, S. Miller, D. Duckworth, H. Hu, A. Wan, X.-Y. Fu, K. Goldberg, and P. Abbeel, "Superhuman performance of surgical tasks by robots using iterative learning from human-guided demonstrations," in *2010 IEEE IROS*, 2010, pp. 2074–2081.

[20] V. Schorp, W. Panitch, K. Shivakumar, V. Viswanath, J. Kerr, Y. Avigal, D. M. Fer, L. Ott, and K. Goldberg, "Self-supervised learning for interactive perception of surgical thread for autonomous suture tail-shortening," in *2023 IEEE 19th CASE*, 2023, pp. 1–6.

[21] J. Curlin and C. K. Herman, "Current state of surgical lighting," *Surg. J.*, vol. 6, no. 2, pp. e87–e97, Apr. 2020.

[22] L. Lipson, Z. Teed, and J. Deng, "Raft-stereo: Multilevel recurrent field transforms for stereo matching," 2021.

[23] D. Cohen-Steiner and F. Da, "A Greedy Delaunay Based Surface Reconstruction Algorithm," INRIA, Tech. Rep. RR-4564, Sept. 2002.

[24] T. Y. Zhang and C. Y. Suen, "A fast parallel algorithm for thinning digital patterns," *Commun. ACM*, vol. 27, no. 3, p. 236–239, mar 1984.

[25] P. Dierckx, *Curve and surface fitting with splines*, ser. Numerical Mathematics and Scientific Computation. Oxford, England: Clarendon Press, Apr. 1995.

[26] D. L. Dunn, Ed., *Ethicon Wound Closure Manual*. Ethicon, Incorporated, 1994.

[27] D. Kraft, "A software package for sequential quadratic programming," *Forschungsbericht- Deutsche Forschungs- und Versuchsanstalt fur Luft- und Raumfahrt*, 1988.

[28] U. Devgan, "Basic principles of ophthalmic suturing," https://cataractcoach.com/2018/07/29/basic-principles-of-ophthalmic-suturing/, accessed: 2023-03-12.